Coupled Simulation of Two-Dimensional Hybrid Hall Thruster Models

IEPC-2019-318

Presented at the 36th International Electric Propulsion Conference
University of Vienna, Austria
September 15-20, 2019

Rei Kawashima,* Junhwi Bak,† Yushi Hamada,‡ Bastiaan Van Loo,§
Hiroyuki Koizumi,¶ and Kimiya Komurasaki‖
The University of Tokyo, Tokyo, 113-8656, Japan

Abstract: A coupled simulation of axial-azimuthal (Z-θ) and axial-radial (Z-R) two-dimensional models is proposed for a self-consistent simulation of the Hall thruster discharge. The Z-θ model simulates azimuthal plasma oscillations to obtain an anomalous electron transport property. The Z-R model simulates the thruster performance, ion wall fluxes, and effects of magnetic field geometry. To examine the validity of the model, the coupled Z-θ-Z-R simulation is applied to a thruster with anode layer (TAL) UT-58 and a stationary plasma thruster (SPT) SPT-100. The results of the Z-θ simulation show that azimuthal plasma oscillations exist and these oscillations enhance the cross-field electron transport, especially in the plume region. In the TAL case, the axial distribution of simulated plasma potential agrees with the emissive probe measurement data, indicating the validity of the simulated electron transport property. Concerning the SPT case, the effective electron mobility obtained from the simulation qualitatively agrees with the empirical distributions. In addition, the mesh convergence is confirmed in the anomalous electron mobility property and space potential distribution. The Z-R simulations successfully run with the anomalous electron mobility properties obtained in the Z-θ simulations, in both the TAL and SPT cases. The predicted discharge currents are close to the experimental results in both the TAL and SPT cases, which supports the validity of the simulated electron transport properties. The validity of the Z-θ-Z-R coupled simulation for the self-consistent Hall thruster discharge model is shown.

Nomenclature

B	= magnetic flux density	i_e	= electron internal energy
j_e	= electron current density	k	= reaction rate coefficient
L_c	= discharge channel length	M	= magnetization tensor
n_e	= electron number density	T_e	= electron temperature
u_e	= electron velocity	α_B	= Bohm diffusion coefficient
α_E	= energy loss coefficient	ϕ	= space potential
ν	= collision frequency	μ_e	= electron mobility
Ω	= electron Hall parameter		
Subscripts			
col	= collision	eff	= effective
ion	= ionization	mom	= momentum exchange

*Assistant Professor, Department of Aeronautics and Astronautics, kawashima@al.t.u-tokyo.ac.jp.
†Graduate Student, Department of Aeronautics and Astronautics.
‡Graduate Student, Department of Advanced Energy.
§Graduate Student, Department of Aeronautics and Astronautics.
¶Associate Professor, Department of Advanced Energy.
‖Professor, Department of Aeronautics and Astronautics.

I. Introduction

NUMERICAL modeling technology of Hall thrusters has been advanced and the computer-aided-engineering (CAE) is used in the development process of Hall thrusters. In the design processes of recent stationary plasma thruster (SPT), numerical analyses are preceding the actual thruster manufacturing.[1,2] On the other hand, Japanese universities conduct a collaborative project to develop a high-performance thruster with anode layer (TAL).[3] The 5 kW-class RAIJIN66 thruster developed in this project achieved a high performance that was competitive with the performances of SPT-type thrusters in the same power level. A high-fidelity numerical simulation is envisaged for TALs to develop further high-performance thrusters.

One of the remaining issues in the numerical simulation of Hall thruster is the self-consistent modeling of the cross-field electron transport. It is well known that the discharge current and plasma property distribution observed in experiments cannot be reproduced by numerical simulation if one assumes only the classical diffusion. In the axisymmetric modeling of Hall thrusters, a numerical solution of stable plasma discharge cannot be obtained with only the classical diffusion.[4] Hence it has been necessary to add an ad-hoc function for the "anomalous" part in the cross-field electron mobility. For SPTs, there have been several works about the empirical expression for the anomalous electron transport.[5,6] However, in TALs, there have been little experimental data about the anomalous electron transport characteristics, and an empirical model is not available. In fact, the issue of anomalous electron transport have been found in other plasma sources with E×B configurations such as HiPIMS,[7] and this issue entails a general scientific concern. The characteristics of anomalous electron transport must be included in the model by a self-consistent manner, to achieve high-fidelity numerical simulations for SPT, TAL, and other E×B plasma sources.

One hypothesis for the mechanism of anomalous electron transport is related to plasma oscillations in the azimuthal (E×B) direction. In brief, this mechanism requires the three properties to increase the electron flux toward the anode as follows: 1) azimuthal oscillation in plasma potential, 2) azimuthal oscillation in electron density, and 3) out-of-phese between the plasma potential and electron density. The property 1) is required to induce the $E_\theta \times B_r$ drift of electron motion in the axial direction. The properties 2) and 3) are required to increase the net electron flux toward the anode when the axial electron flux is integrated in azimuth. The oscillation types to account for the anomalous electron transport may be the low-frequency (∼tens of kHz) rotating spoke or the high-frequency (∼MHz) electron cyclotron drift oscillation. A lot of experiments, numerical simulations, and linear stability analyses have been conducted to investigate the characteristics of these oscillations. In both the rotating spoke and electron cyclotron drift oscillation, the abovementioned three properties have been observed in experiments and numerical simulations.

The calculation of azimuthal plasma oscillations would be the key to achieve the Hall thruster discharge simulation with a self-consistent electron transport model. A pioneering research for the self-consistent simulation of Hall thruster discharge was done by Hirakawa.[8,9] A full particle-in-cell (PIC) simulation was performed in the R-θ plane, and a plasma fluctuation was found in the azimuthal direction. It was reported that the azimuthal electric field induced by the oscillation increased the cross-field electron mobility, and this effect was greater than the effect of secondary-electron emission from the wall surface. In addition, a Z-R full-PIC simulation was attempted by using the information of anomalous electron transport obtained by the R-θ simulation. Lopez Ortega et al. presented the results of self-consistent model in which the wave action equation was coupled with the Z-R multi-fluid model called the Hall2De.[10] The evolution of the wave action was calculated based on the ion acoustic instability, and the anomalous collision frequency was evaluated from the wave action equation. It was reported the the potential distribution obtained in this simulation agreed well with the profile inferred from experimental measurements.

We present a coupled simulation of Z-θ and Z-R two-dimensional models for the self-consistent simulation of the Hall thruster discharge. The concept of the Z-θ-Z-R coupled simulation is shown in Fig. 1. The purpose of the Z-θ simulation is to analyze the azimuthal plasma oscillation and to obtain the property of anomalous electron transport. The information of oscillation-induced electron transport is obtained based on the Z-θ calculation result, and this information is used in the Z-R simulation to include the effects of anomalous electron transport. The Z-R simulation predicts the thruster performance and the effect of the 2D magnetic field geometry. In addition, the ion losses to the channel walls are calculated in the Z-R simulation, and this profile is then used in the Z-θ simulation to include the ion wall loss effects. By continuing the iteration of Z-θ and Z-R calculations until a quasi-steady state is reached, a self-consistent plasma flow simulation that considers both the oscillation-induced electron transport and ion wall losses is attained. We adopt a particle-fluid hybrid model for both the Z-θ and Z-R simulations.

In this study, the Z-θ-Z-R simulation is applied to the very different two cases: TAL UT-58 and SPT-100.

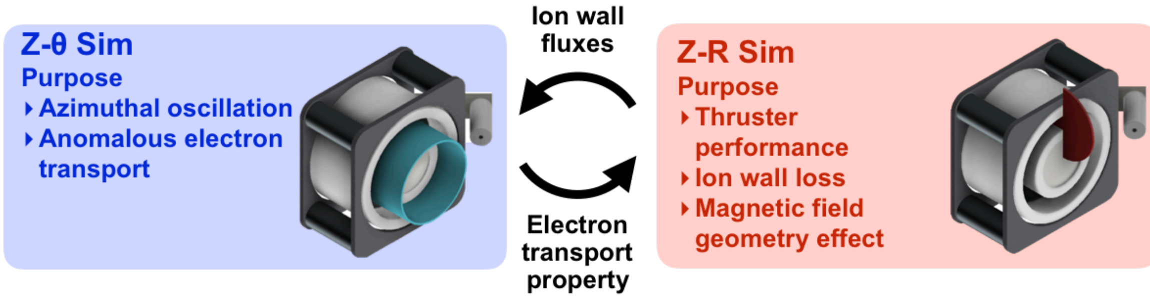

Figure 1. Concept of the coupled Z-θ-Z-R simulation.

The results of plasma oscillation analyses and anomalous electron transport properties are presented for the two cases. The validity of the model is examined by comparing the simulation results with the experimental data.

II. Two-Dimensional Particle-Fluid Hybrid Model

II.A. Ion and Neutral Particles

The ion and neutral particle flows are calculated by the particle model. The motion of equation is solved for each macroparticle of ions and neutral particles. Ions are accelerated by the electric field, neglecting the effect of magnetic field. Neutral particle motions are the free movement.

Inter-particle collisions between heavy particles are neglected for simplicity. In addition, the present model handles only single ions generated by the electron-neutral collisional ionization process. The charge-exchange collision (CEX) process is also ignored. Electron-neutral momentum-exchange collision and ionization collision are calculated by assuming the Maxwellian distribution in the electron energy. The momentum-exchange collision frequency and ionization collision frequency are respectively written as follows:

$$\nu_{\mathrm{mom}} = n_{\mathrm{n}} k_{\mathrm{mom}}, \qquad \nu_{\mathrm{ion}} = n_{\mathrm{n}} k_{\mathrm{ion}}. \tag{1}$$

k_{mom} and k_{ion} are the reaction rate coefficients, and emprical expressions of these coefficients in Ref. 11 are used in this study. When ions and neutral particles collide with the anode or channel wall, they are reflected diffusively after losing their charge.

The advancement of each particle is implemented by the leap-frog method, which is second-order time accurate. A linear function is used in the particle-to-cell and node-to-particle weighting processes. The time step interval is set as 2.0 ns in the Z-θ simulation and 5.0 ns in the Z-R simulation. The number of macroparticles is adjusted to make each cell contains $\sim$200 macro particles on average, and usually several hundred millions of macro particles flow in the calculation region.

II.B. Electron Mass and Momentum

Two-dimensional conservation equations of mass, momentum, and energy are considered for the electron fluid in quasi-neutral plasmas. In the mass conservation equation, the electron number density is treated as a time-constant distribution by assuming the quasi-neutrality in the electron's time scale. Thus, the mass conservation equation is regarded as the equation of continuity as follows:

$$\nabla \cdot (n_{\mathrm{e}} \vec{u}_{\mathrm{e}}) = n_{\mathrm{e}} \nu_{\mathrm{ion}}. \tag{2}$$

Conservation of the electron momentum is derived by assuming inertialess electrons, as follows:

$$-n_{\mathrm{e}} \nabla \phi + \nabla (n_{\mathrm{e}} T_{\mathrm{e}}) = -n_{\mathrm{e}} \nu_{\mathrm{col}} [M] \vec{u}_{\mathrm{e}}. \tag{3}$$

Here $[M]$ is named the magnetization tensor, and the expression for this tensor is discussed in the next section.

In conventional approaches, Eq. (2) and Eq. (3) are integrated into an elliptic equation to solve for the space potential.[12] It has been reported that there is a numerical instability in the potential solver for the axial-azimuthal coordinate.[13] It is known that the potential solver becomes an anisotropic diffusion problem if the electrons are strongly magnetized.[14] It is difficult to maintain a stability while computing this equation because the cross-diffusion terms cause failure of the diagonal dominance of the coefficient matrix.

Alternatively, the hyperbolic-equation system approach using pseudo-time advancement terms is considered. This approach has been developed for robust computation of magnetized electron fluids. The processes for deriving the hyperbolic system were presented elsewhere.[15,16] A second-order upwind method using the total variation diminishing monotonic upwind scheme for conservation laws (TVD-MUSCL) technique with the minmod limiter function, is used for the space discretization. In the sub-loop for the electron mass and momentum equations, the calculation must be continued until a steady-state is reached, since the electron mass and momentum equations are regarded as time-independent equations. In the hyperbolic system approach, a preconditioning technique is designed to avoid the numerical stiffness and to accelerate the convergence. Time integration is implemented by using an efficient multidimensional implicit method based on the alternating-direction-implicit symmetric Gauss-Seidel (ADI-SGS) method.[17]

II.C. Electron Energy

In the electron energy conservation equation, the kinetic energy part is neglected, and the conservation of electron internal energy is considered. The conservation equation for the internal energy is written as follows:

$$\frac{\partial}{\partial t}\left(\frac{3}{2}en_{\mathrm{e}}T_{\mathrm{e}}\right)+\nabla\cdot\left(\frac{5}{2}en_{\mathrm{e}}T_{\mathrm{e}}\vec{u}_{\mathrm{e}}-\frac{5}{2}en_{\mathrm{e}}T_{\mathrm{e}}\left[\mu\right]\nabla T_{\mathrm{e}}\right)=en_{\mathrm{e}}\vec{u}_{\mathrm{e}}\cdot\nabla\phi-\alpha_{\mathrm{E}}e\varepsilon_{\mathrm{ion}}n_{\mathrm{e}}\nu_{\mathrm{ion}}. \tag{4}$$

α_{E} is the coefficient to handle the energy losses of ionization, excitation, and radiation with single term. This coefficient is experimentally determined as a function of electron temperature.[18]

In the Z-θ simulations, the electron energy equation is calculated only in the axial direction, and electron temperature is assumed to be symmetric in the azimuthal direction. Two-dimensional plasma properties such as the ion density and neutral density are averaged in the azimuthal direction to produce axial distributions. These axial distributions are used in the calculation of the axial 1D electron energy conservation equation. On the other hand, in the Z-R simulations, the energy conservation equation is calculated in 2D, with the 2D tensor of the heat conductivity. In the calculation of Eq. (4), the time integration is implemented by using a first-order fully implicit method incorporated with the direct matrix inversion method. The electron energy equation is handled as time-dependent, and the time step is typically set as 1.0×10^{-10} s in the Z-θ simulation and 5.0×10^{-10} s in the Z-R simulation.

II.D. Electron Mobility

In the electron fluid model, the effect of magnetic confinement is expressed by the electron mobility tensor $[\mu]$. The electron mobility tensors for the Z-θ and Z-R coordinates are respectively expressed as follows:

$$[\mu]_{z-\theta}=\frac{\mu_{\mathrm{e}}}{1+\Omega^2}\begin{bmatrix}1 & \Omega\\ -\Omega & 1\end{bmatrix}. \tag{5}$$

$$[\mu]_{z-r}=\frac{\mu_{\mathrm{e}}}{1+\Omega^2}\begin{bmatrix}1+\Omega_z^2 & \Omega_z\Omega_r\\ \Omega_z\Omega_r & 1+\Omega_r^2\end{bmatrix}. \tag{6}$$

μ_{e} is the mobility of unmagnetized electrons written as $\mu_{\mathrm{e}}=e/m_{\mathrm{e}}\nu_{\mathrm{col}}$, and Ω is the electron Hall parameter defined as $\Omega=\mu_{\mathrm{e}}B$. The electron Hall parameters for the z- and r-directions are defined as $\Omega_z=\mu_{\mathrm{e}}B_z$ and $\Omega_r=\mu_{\mathrm{e}}B_r$. The original definition of the Hall parameter is the ratio of gyrofrequency to collision frequency, and the Hall parameter does not have the directionality. Here Ω_z and Ω_r are used for the convenience of formulation. The magnetization tensor $[M]$ in Eq. (3) has a relation with the electron mobility as $[M]=\mu_{\mathrm{e}}\left[\mu\right]^{-1}$.

In the Z-θ simulation, only the classical diffusion is used for the cross-field electron transport. Thus, the collision frequency in the electron mobility is assumed to be the same as the electron-neutral momentum-exchange collision frequency.

$$\nu_{\mathrm{col},z-\theta}=\nu_{\mathrm{mom}}. \tag{7}$$

On the other hand, the anomalous electron transport must be assumed in the Z-R simulation. Referring to the previous numerical models,[19,20] the Bohm diffusion model is used for the anomalous electron transport. The collision frequency for the Z-R simulation is modeled as follows:

$$\nu_{\mathrm{col},z-r} = \nu_{\mathrm{mom}} + \nu_{\mathrm{B}} = \nu_{\mathrm{mom}} + \frac{\alpha_{\mathrm{B}}}{16} \cdot \frac{eB}{m_{\mathrm{e}}}, \tag{8}$$

where α_{B} is the Bohm diffusion coefficient. There have been several researches on the empirical expression for α_{B}. A common method is to vary the coefficient as a function of axial position. Detailed analyses comparing simulations and experiments have revealed that α_{B} typically has a small value of ~ 0.1 inside the discharge channel and relatively large value of ~ 1.0 in the plume region, in the cases of SPT-type thrusters. For TAL-type thrusters, there have been few researches about the expression of the anomalous electron transport. In this study, the anomalous electron transport property is evaluated by the Z-θ simulation, and the distribution of α_{B} is obtained. The obtained α_{B} is then used in the Z-R simulation.

III. Case TAL, Z-θ Simulation

III.A. Calculation Condition

In this case, a TAL-type thruster UT-58 is assumed as the calculation target. The detail of the thruster design and performance can be found in Ref. 21. The parameters of thruster operation condition is presented in Table 1. Relatively low discharge voltage and mass flow rate are assumed in this simulation. This is because the thruster operation was stable in the experiment with this condition, and a fair comparison between the time-averaged quantities in the simulation and experiment is possible.

Figure 2 shows the calculation region, boundary condition, and axial distribution of magnetic flux density. The hollow anode is often used in TALs to stabilize the discharge, and it is known that some discharge plasmas exist inside the hollow anode. Hence the calculation region is taken to cover both the inside of hollow anode and plume region, as shown in Fig. 2(a). Here $x = 0$ mm is defined by the hollow anode tip.

In the present simulation a full cylinder of the channel centerline is taken for the Z-θ simulation. The cylinder is unwrapped to make a x-y two-dimension plane for the calculation domain, as shown in Fig. 2(b). The neutral particles of propellant gas are introduced into the calculation domain from the anode boundary. At the anode boundary, a Dirichlet condition of the discharge voltage is directly imposed. Here the effect of the anode sheath is ignored because the purpose of this model is to simulate the plasma oscillation in the bulk plasma. The potential at the cathode boundary is assumed based on experimental results. Periodic boundary condition is applied at the top and bottom boundaries in both the particle and electron fluid models. A grid of 48×96 is used as the nominal case in the present analysis.

A measurement of radial magnetic flux density was performed in the region of -5 mm $< x <$ 30 mm. The magnetic field distribution is assumed based on this measurement data. Further, the magnetic field is assumed to be symmetric in the y-direction.

III.B. Plasma Property Distribution

The plasma property distributions obtained from the Z-θ simulation are shown in Fig. 3. The main ionization region exists at around the hollow anode and channel exit, where the neutral particle density steeply decreases. The neutral particle density is almost uniform in the azimuthal direction. If a rotating spoke

Table 1. The input parameters assumed in the TAL-case simulation.

Parameter	Value
Mass flow rate	2.04 mg/s
Discharge voltage	150 V
Channel centerline diameter	58 mm
Channel width	8 mm
Anode temperature	650 K

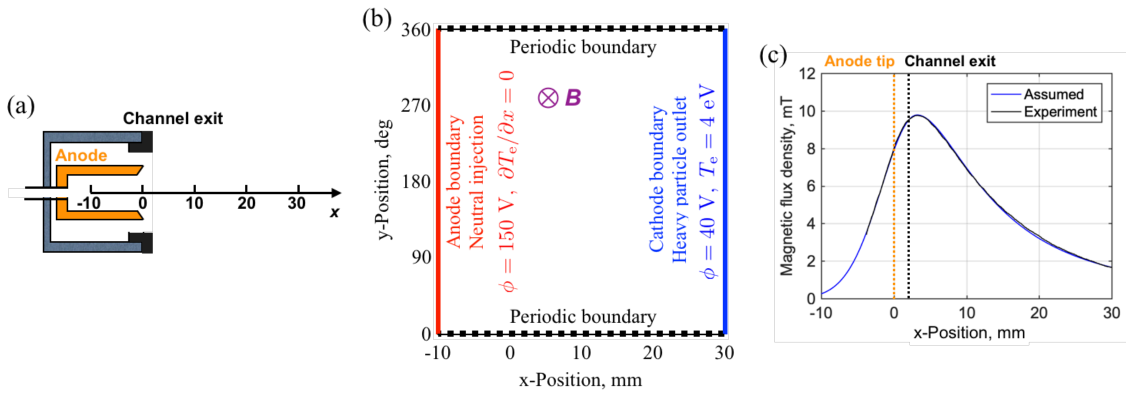

Figure 2. Calculation condition for the Z-θ simulation; (a) relationship between the calculation region and channel, (b) calculation domain and boundary conditions, and (c) axial distribution of the radial magnetic flux density.

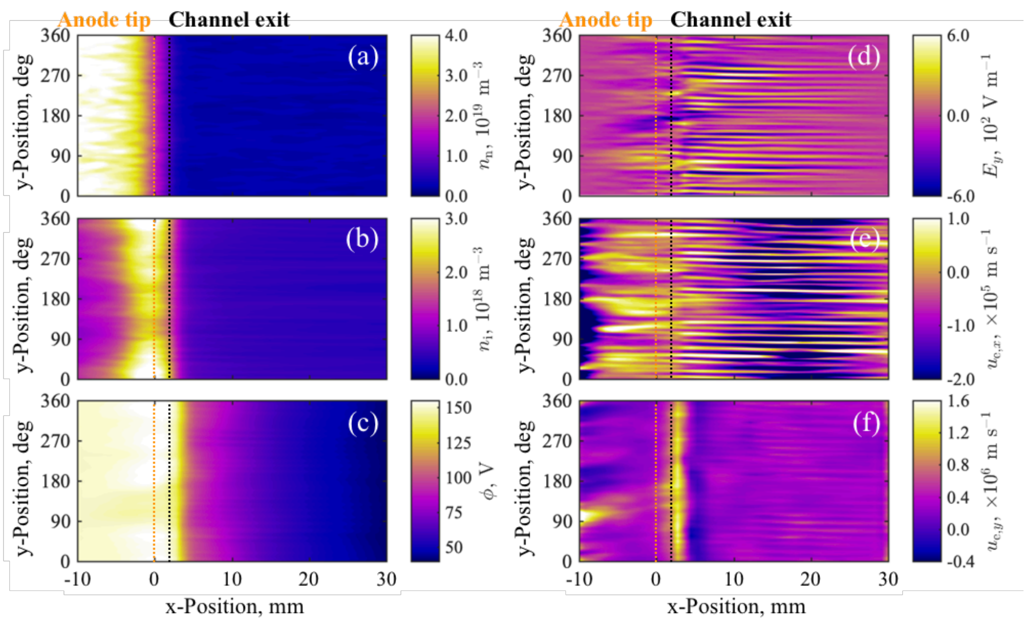

Figure 3. Plasma property distributions obtained from the Z-θ simulation; (a) neutral number density, (b) ion number density, (c) space potential, (d) y-electric field, (e) x-electron velocity, and (f) y-electron velocity.

appears, an azimuthal inhomogeneity appears in the neutral particle density.[22] Thus, azimuthally uniform n_n in the present simulation result indicates that there is no rotating spoke. The peak of ion number density is at around the hollow anode tip, and some fraction of ions are included inside the hollow anode. The space potential is close to the anode voltage inside the hollow anode. The main acceleration region exists just downstream of the discharge channel exit.

Azimuthal fluctuations are observed in the ion number density and space potential distributions, especially in the plume region around $x = 10$ mm. A fast Fourier transform analysis indicates that the wavelength of this oscillation is 7.6 mm. A steady propagation of coherent structure is hardly observed in the present simulation results, and hence the propagation velocity and frequency are unclear. The azimuthal oscillation amplitude in the space potential at $x = 10$ mm is ~ 2 V, which results in the azimuthal electric field up to 10^3 V/m. Owing to the E×B effect, the axial electron velocity also shows oscillatory distribution.

The observed wavelength is large compared with the typical wavelength of electron drift instability.[23] Since the hybrid model is capable of simulating the gradient drift instabilities, it is inferred that the azimuthal oscillation shown in this study is one of the gradient drift instabilities. A comparison between the numerical simulation and linear stability analysis based on the drift instabilities[24,25] may be useful in detecting the type of the azimuthal oscillation. This is one of the themes of subsequent works.

III.C. Effective Electron Mobility Analysis

The influence of the azimuthal plasma oscillation on the axial electron current and cross-field electron mobility is investigated. Since both the n_e and ϕ are fluctuating, the net electron current in the axial direction can be affected by the oscillation, if there exists an out-of-phase between n_e and ϕ. In the Z-θ simulation, the electron current density in the x-direction is written as the summation of the diffusion and drift currents, as follows:

$$\begin{aligned} j_{\mathrm{e},x} &= j_{\mathrm{e},x,\mathrm{diffusion}} + j_{\mathrm{e},x,\mathrm{drift}} \\ &= -\frac{1}{1+\Omega^2} e\mu_\mathrm{e} \left(n_\mathrm{e} \frac{\partial \phi}{\partial x} - \frac{\partial}{\partial x}\left(n_\mathrm{e} T_\mathrm{e}\right) \right) - \frac{\Omega}{1+\Omega^2} e\mu_\mathrm{e} \left(n_\mathrm{e} \frac{\partial \phi}{\partial y} - \frac{\partial}{\partial y}\left(n_\mathrm{e} T_\mathrm{e}\right) \right) \end{aligned} \tag{9}$$

Note that x- and y-directions correspond to axial and azimuthal directions, respectively. Here the $j_{\mathrm{e},x,\mathrm{diffusion}}$ and $j_{\mathrm{e},x,\mathrm{drift}}$ are defined by the x-electron current densities induced by the x-gradients and y-gradients, respectively.

The effects of the diffusion and drift terms on the total electron current are analyzed. The axial distributions of azimuthally averaged quantities $\langle j_{\mathrm{e},x} \rangle$, $\langle j_{\mathrm{e},x,\mathrm{diffusion}} \rangle$, and $\langle j_{\mathrm{e},x,\mathrm{drift}} \rangle$ are plotted in Fig. 4. If one looks at the $j_{\mathrm{e},x}$, the value on the right-hand side boundary corresponds to the electron current flowing into the discharge channel from the cathode. The electrons flow toward the anode with conserving the electron current in the plume region. At the region around the channel exit, the $j_{\mathrm{e},x}$ increases owing to the ionization. The $j_{\mathrm{e},x}$ on the left-hand side boundary corresponds to the discharge current. $j_{\mathrm{e},x,\mathrm{diffusion}}$ is close to the $j_{\mathrm{e},x}$ inside the channel, which means that the diffusion effect is predominant in the discharge channel. On the other hand, $j_{\mathrm{e},x,\mathrm{diffusion}}$ is much less than $j_{\mathrm{e},x}$ in the plume region. This is because the neutral number density becomes small in the plume region, and the classical diffusion cannot carry the electron current. The $j_{\mathrm{e},x,\mathrm{drift}}$ starts increasing just downstream of the channel exit, and it becomes close to the $j_{\mathrm{e},x}$ in the plume region. The location of $j_{\mathrm{e},x,\mathrm{drift}}$ increase corresponds to the region where the azimuthal plasma oscillation starts. It is found that the azimuthal plasma oscillation induces the electron drift current, and the drift effect enhances the cross-field electron transport, especially in the plume region.

The main purpose of the Z-θ simulation is to obtain the anomalous electron mobility property. As well as the preceding researches, the effective electron mobility is used for the analysis. The effective electron mobility μ_eff is defined as follows:

$$\langle j_{\mathrm{e},x} \rangle = -e\mu_\mathrm{eff} \left\langle n_\mathrm{e} \frac{\partial \phi}{\partial x} - \frac{\partial}{\partial x}\left(n_\mathrm{e} T_\mathrm{e}\right) \right\rangle . \tag{10}$$

If one attributes the diffusion and drift electron currents to only the x-(axial) gradients, the μ_eff appears. The effective electron mobility calculated for the present simulation is plotted in Fig. 5, and compared with the electron mobility of the classical diffusion. Inside the hollow anode, the effective electron mobility was close to the classical mobility. On the other hand, the electron transport was enhanced in the plume region, and the effective electron mobility was greater than the classical mobility by one to two orders of magnitude. It is concluded that the plasma oscillation increases the cross-field electron mobility, by one to two orders of magnitude.

In the Z-R axisymmetric simulations for Hall thrusters, the anomalous electron transport property is often modeled by assuming the Bohm diffusion, as written in Eq. (8). The Bohm diffusion coefficient α_B is an arbitrary coefficient. Here the axial distribution of α_B is assumed as follows:

$$\alpha_\mathrm{B} = \left(\alpha_\mathrm{p} - \alpha_0\right) \frac{1}{2} \left(1 + \mathrm{erf}\left(\frac{1}{2\sigma^2} \cdot \frac{x - x_\mathrm{p}}{L_\mathrm{c}} \right) \right) + \alpha_0, \tag{11}$$

where the parameters are set as

$$\alpha_0 = 1.0, \qquad \alpha_\mathrm{p} = 0.1, \qquad x_\mathrm{p} = 6.5\ \mathrm{mm}, \qquad \sigma = 0.08. \tag{12}$$

This function gives $\alpha_\mathrm{B} = 1.0$ in the plume region of $x > 10$ mm, and $\alpha_\mathrm{B} = 0.1$ inside the channel. The electron mobility corresponding to the Bohm diffusion model is also plotted in Fig. 5. In the plume region, the effective electron mobility obtained from the simulation is close to the so-called Bohm diffusion of $\mu_\mathrm{eff} = 1/16B$. The physical background for this agreement is being investigated. The azimuthal oscillation amplitude is related to the axial electron transport. Thus, it is inferred that the oscillation growth is saturated when the axial electron transport becomes similar to the Bohm diffusion.

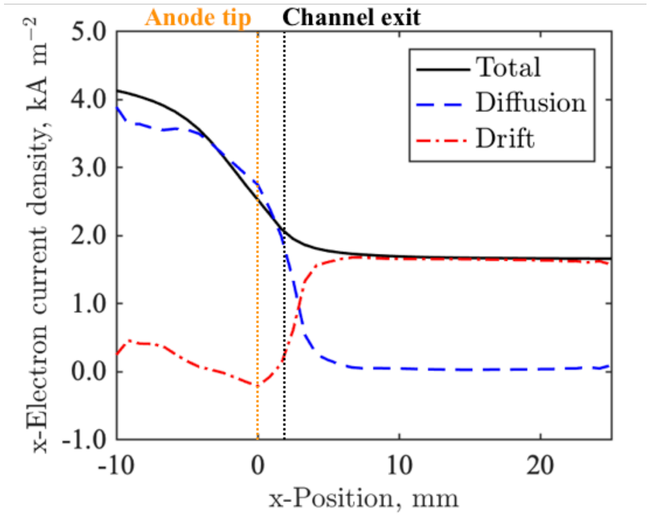

Figure 4. Azimuthally averaged electron current densities of total ($j_{e,x}$), diffusion ($j_{e,x,\mathrm{diffusion}}$), and drift ($j_{e,x,\mathrm{drift}}$) in the x-direction.

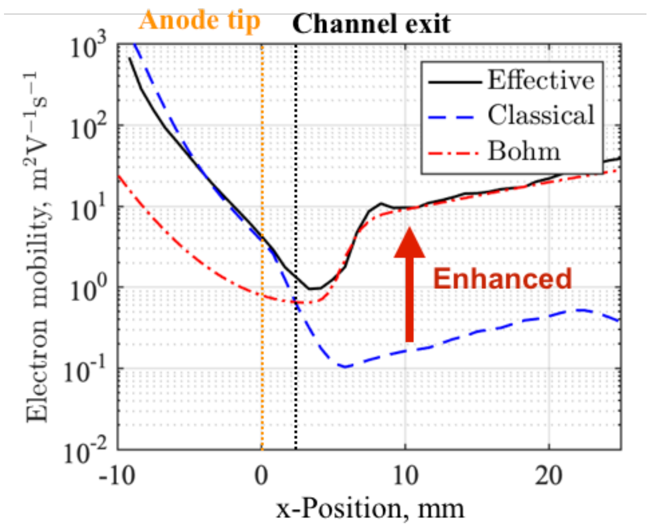

Figure 5. Comparison of axial distributions of the effective electron mobility and the electron mobility based on classical diffusion. The approximation by the Bohm diffusion model is also plotted.

III.D. Validation of Simulation Results

The validity of the Z-θ simulation results is checked by comparing the simulated space potential distribution with experiment and confirming the mesh convergence. The influence of the effective electron mobility is directly reflected to the space potential distribution. Hence the space potential distributions are compared between the simulation and experiment to validate the effective electron mobility property obtained in the Z-θ simulation. As the experimental data, the plasma potential distribution on the channel centerline was measured by an emissive probe.[26] A spatially continuous data was obtained by applying the floating potential method in the emissive probe.

The comparison of plasma potential distributions on the channel centerline is presented in Fig. 6. Note that the plasma potential is given at both the left- and right-hand side boundaries in the simulation. Overall, a good agreement is observed between the simulation and experiment. Inside the hollow anode, the plasma potential is almost flat and close to the anode potential. The potential gradient between the anode tip and channel exit is moderate, and about 90% of the discharge voltage is maintained at the channel exit. The calculation target, UT-58, is a TAL with a short discharge channel length and channel wall at cathode

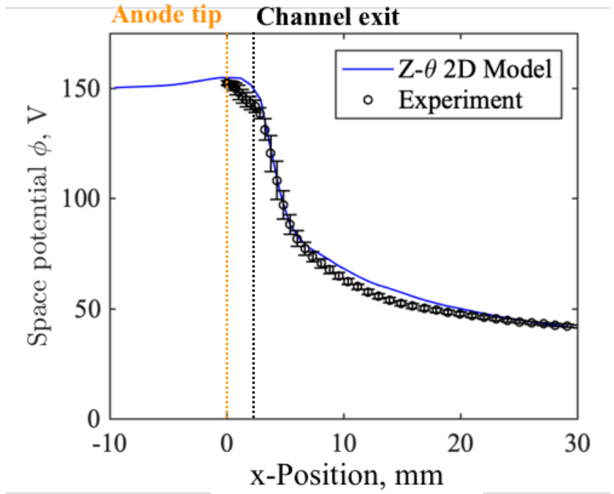

Figure 6. Comparison of axial distributions of space potential between the Z-θ simulation and emissive probe measurement.

potential. However, the so-called "anode layer" is not formed. This is because the magnetic field is designed to generate the plasma lens effect and to reduce the plasma-wall interaction. An electrostatic sheath of large potential drop is formed in front of the guard ring (channel wall). Owing to this strong sheath, the plasma potential is maintained high in the vicinity of the channel exit. The main acceleration region exists just downstream of the channel exit, and a close match is observed between the simulation and experiment about the location of the acceleration region. Based on the agreement in the plasma potential distributions, it is concluded that the electron transport property obtained from the Z-θ simulation is valid.

Since the effect of electron transport enhancement is caused by the azimuthal plasma oscillation in the Z-θ simulation, the mesh should be fine enough to obtain accurate anomalous electron transport property. The azimuthal grid resolution is concerned for the anomalous electron mobility analysis. Here, the mesh convergence of the effective electron mobility and space potential distribution have been checked by varying the mesh as 48×60, 48×72, 48×96, and 48×128. The results of different grid systems are presented in Fig. 7. The effective electron mobility inside the channel is almost unchanged when the grid system is varied. This fact means that the neutral particle density is not affected by the grid resolution, because the electron transport inside the channel is mainly governed by the classical diffusion.

On the other hand, the effective electron mobility in the plume region increases when the number of azimuthal grid points increases. The effect of electron transport enhancement owing to azimuthal plasma oscillation becomes more significant in the fine grid systems. If one looks at the value at $x = 7$ mm, the difference between the electron mobilities of 48×96 and 48×120 cases is small. Hence, it is concluded that a mesh convergence is attained in the effective electron mobility with the 48×96 grid.

The results of space potential also indicate that the 48×96 grid yields a converged result. In the result of 48×60, the potential drop in the main acceleration region is less steeper than the experimental result. When the number of grid points is increased, the potential drop becomes steeper, and the results of 48×96 and 48×120 cases are very similar to each other. The results of these two cases are close to the experimental result. It is shown that the grid is fine enough to estimate the anomalous electron property accurately.

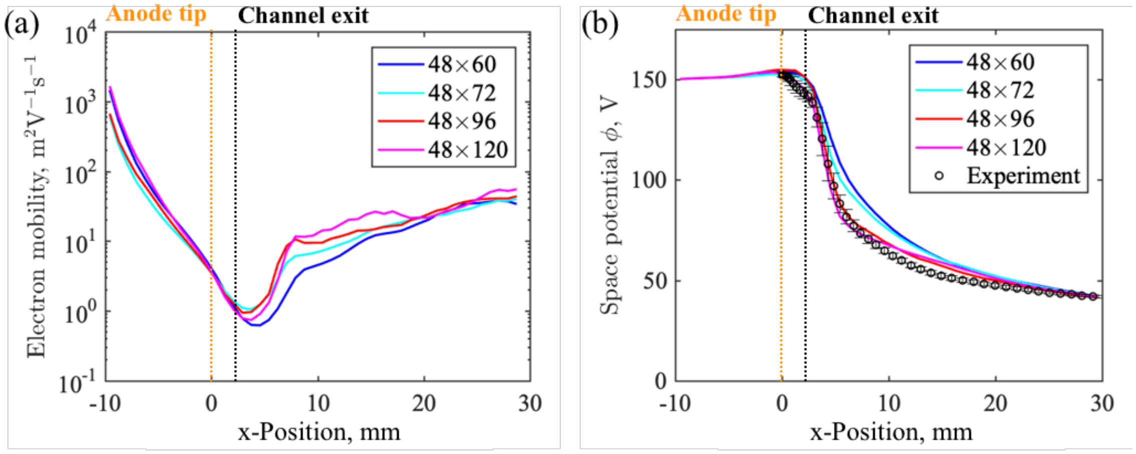

Figure 7. One-dimensional distributions of (a) effective electron mobility and (b) space potential, calculated with different grid systems.

IV. Case TAL, Z-R Simulation

IV.A. Calculation Condition

The calculation domain and boundary conditions are shown in Fig. 8. In this research, only the region of quasineutral plasma is included in the calculation domain. The sheath region in front of the guard rings are not handled. A rectangular region with the radial length of the hollow anode width is used as the calculation domain. The axial length is set to include both the hollow anode and plume regions. The neutral particles are injected into the calculation domain from the left-hand side boundary. The anode potential is set on the boundaries of the hollow anode walls. On the top and bottom boundaries of free space, the neutral atoms and ions flow out, whereas $j_e = 0$ is assumed for the electron fluid calculation. On the right-hand side boundary $\phi = 40$ V is assumed based on the experimental data. In this simulation the effect of anomalous electron transport property is considered by using the Bohm diffusion model, where the Bohm diffusion coefficient is given by Eq. (11).

IV.B. Z-R Simulation Results

The Z-R simulation successfully ran for a long time exceeding 1 ms, with the anomalous electron mobility property obtained from the Z-θ simulation. Time histories of thrust and discharge current are shown in Fig. 9. A breathing-mode oscillation with a frequency on the order of 10 kHz is observed. An oscillation with a higher frequency on the order of 100 kHz is also observed, and this oscillation is considered to be the ion-transit oscillation.

The time-averaged thrust and discharge current are compared with the experimental results in Table 2. The thrust is underestimated in the simulation. The reason for this underestimation is supposed to be the inaccurate ion acceleration calculation in the plume region, because of the narrow calculation region in the radial direction. On the other hand, the simulated discharge current is close to the measurement result. Since the discharge current is closely related to the cross-field electron transport, this agreement supports the validity of the anomalous electron transport property obtained in the Z-θ simulation.

The plasma property distributions obtained by the Z-R simulation are shown in Fig. 10. Both the electron density and ionization rate peaks exist around the channel exit. In the UT58, owing to the short discharge channel length and tailored magnetic field, the main ionization region is moved to downstream, compared with typical SPT-type thrusters. The peak of electron temperature is about 26 eV, which is relatively high considering the discharge voltage of 150 V. The high electron temperature is associated with the TAL characteristics of the metallic channel wall at the cathode potential. Because the heat flux flowing into the channel walls is small in TALs, the electron temperature becomes high.

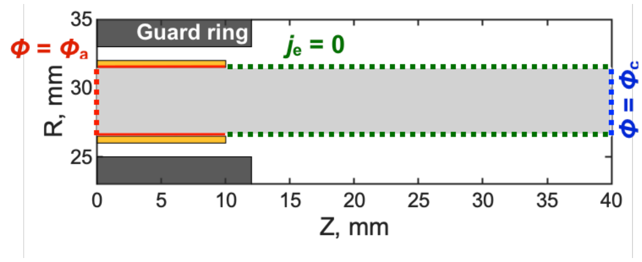

Figure 8. Calculation condition for the Z-R simulation (TAL case). ϕ_a **and** ϕ_c **are 150 V and 40 V respectively, in this study.**

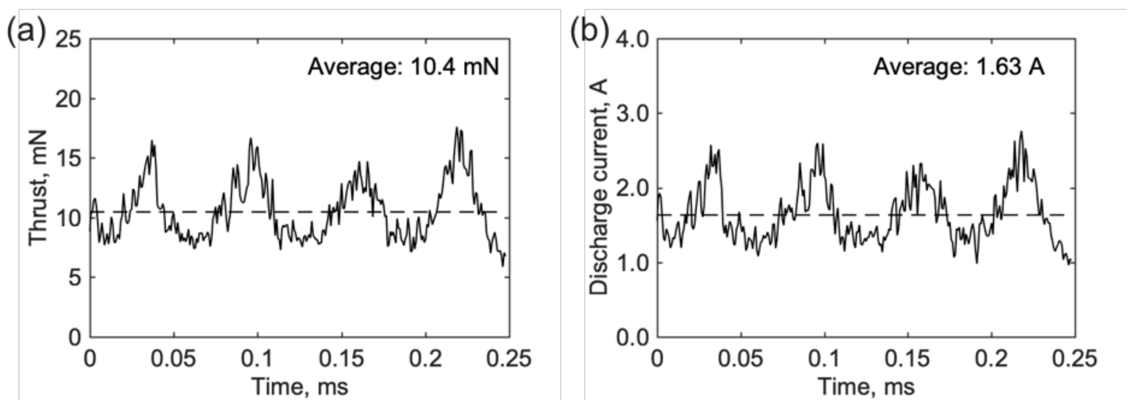

Figure 9. Time histories of thrust and discharge current calculated in the Z-R simulation.

Table 2. Comparison of thrust and discharge current between the Z-R simulation and experiment.

Parameter	Simulation	Experiment
Thurst	10.4 mN	14.9 mN
Discharge current	1.63 A	1.59±0.09 A

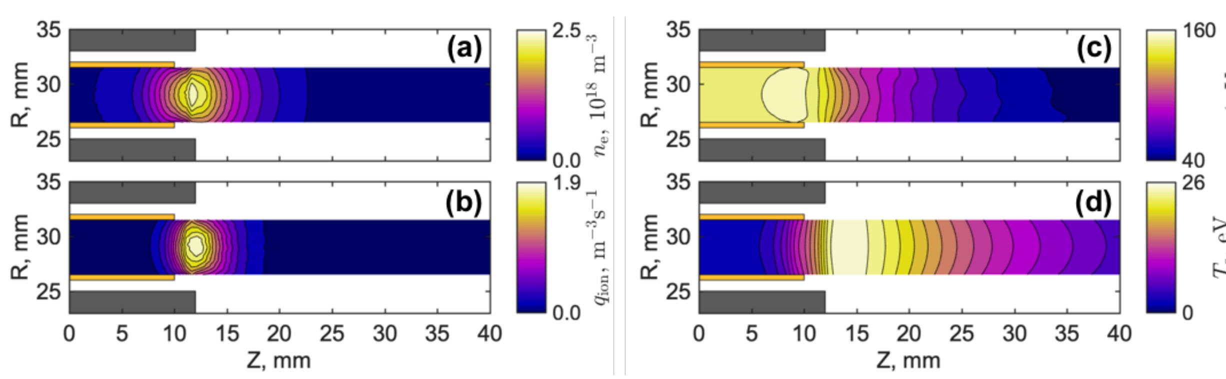

Figure 10. Plasma property distributions obtained from the Z-R simulation for the TAL case; (a) ion number density, (b) ionization rate, (c) space potential, and (d) electron temperature.

V. Case SPT: Z-θ Simulation

V.A. Calculation Condition

The SPT-100 thruster is regarded as a benchmark in the Hall thruster community, and several experiments and numerical simulations have been performed for this thruster. The anomalous electron property has also been investigated, and the nominal thruster performance is known. The applicability of the coupled Z-θ-Z-R simulation is examined by simulating this thruster and validating the simulation results. The parameters for the thruster operation is assumed as Table 3, referring the experimental studies of SPT-100. The magnetic field distribution is assumed by the following equation based on the figures in Ref. 27.

$$B\left(x\right) = B_{\mathrm{p}} \exp\left(-\frac{1}{2\sigma^2}\left(\frac{x}{L_{\mathrm{c}}}-1\right)^2\right), \tag{13}$$

where the parameters are assumed as follows:

$$B_{\mathrm{p}} = 18\ \mathrm{mT}, \qquad \sigma = 0.35\ \ \left(x \leq L_{\mathrm{c}}\right), \quad \sigma = 0.70\ \ \left(x > L_{\mathrm{c}}\right). \tag{14}$$

The appearance of calculation domain for the Z-θ simulation is the same as the one in Fig. 2(b). The azimuthal length of calculation domain corresponds to the full cylinder of channel centerline. The axial length of calculation domain is set as 60 mm where the discharge channel exit is at $x = 23$ mm. The space potential at the anode boundary and cathode boundary are set to 300 V and 0 V, respectively. In this simulation, a rectangular uniform grid of 48×96 points is used.

V.B. Plasma Property Distribution

The plasma property distribution in the Z-θ plane obtained for the SPT case is shown in Fig. 11. As well as the results for the TAL case, azimuthal oscillations are observed in both the electron number density and space potential distributions. The induced azimuthal electric field (E_y) can reach 10^3 V/m, which significantly affects the axial motion of electron fluid. The effect of the plasma oscillation also appears in the azimuthal electron velocity distribution ($u_{\mathrm{e},y}$). The main acceleration region is around the channel exit. A large $u_{\mathrm{e},y}$ is induced in the acceleration region owing to the E×B effect in the azimuthal direction.

The wavelength of the azimuthal oscillation observed in the present simulation is ∼16 mm. This wavelength is large compared with the wavelength of electron cyclotron drift instability observed in the full PIC simulation.[23] In the present study the full cylinder of the channel centerline is taken as the calculation domain and the microscopic plasma oscillations are not directly simulated. It is inferred that both the wavelength and amplitude in the potential fluctuation are large in the present simulation results, and the azimuthal electric field can be large enough to affect the cross-field electron transport.

V.C. Effective Electron Mobility Analysis

The effective electron mobility is evaluated by the method described in Sec. III.C. The effective electron mobility for the SPT case is shown in Fig. 12(a) in comparison with the electron mobility based on the classical diffusion. The cross-field electron transport is greatly enhanced from the classical electron mobility, especially around the channel exit and in the plume region. The effective electron mobility is greater than

Table 3. The input parameters assumed in the SPT-case simulation.[28, 29]

Parameter	Value
Mass flow rate	5.0 mg/s
Discharge voltage	300 V
Outher channel diameter	100 mm
Inner channel diameter	70 mm
Anode temperature	850 K

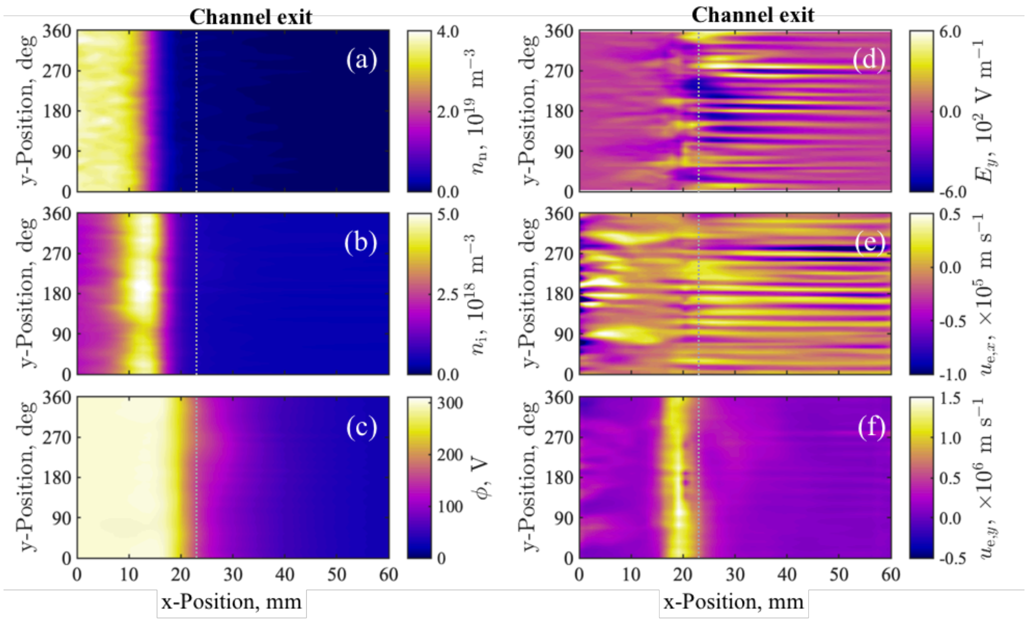

Figure 11. Plasma property distributions obtained from the Z-θ simulation for the SPT case; (a) neutral number density, (b) ion number density, (c) space potential, (d) y-electric field, (e) x-electron velocity, and (f) y-electron velocity.

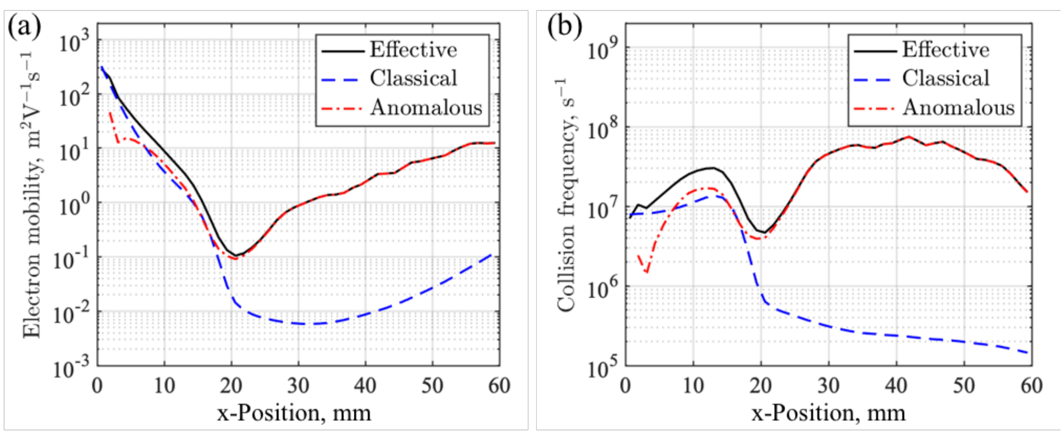

Figure 12. Axial distribution of the (a) effective electron mobility and (b) effective collision frequency. The contributions from the classical and anomalous (oscillation-induced) parts are also plotted.

the classical electron mobility by one or two order of magnitude. As well as the TAL case, the electron transport enhancement is caused by the azimuthal plasma oscillation.

In many numerical models, the effective collision frequency is used in reflecting the anomalous electron transport to the model. The effective collision frequency is calculated from the effective electron mobility as follows:

$$\nu_{\text{eff}} = \frac{e}{m_{\text{e}}}\mu_{\text{eff}}B^2. \tag{15}$$

The axial distribution of the effective collision frequency is shown in Fig. 12(b). The effective collision frequency is also greater than the electron-neutral scattering collision frequency. The effect of classical diffusion is small in the plume region owing to the very sparse neutral atom density. The present simulation clearly shows that the electron transport by the plasma oscillation mainly carries the electron current in the plume region.

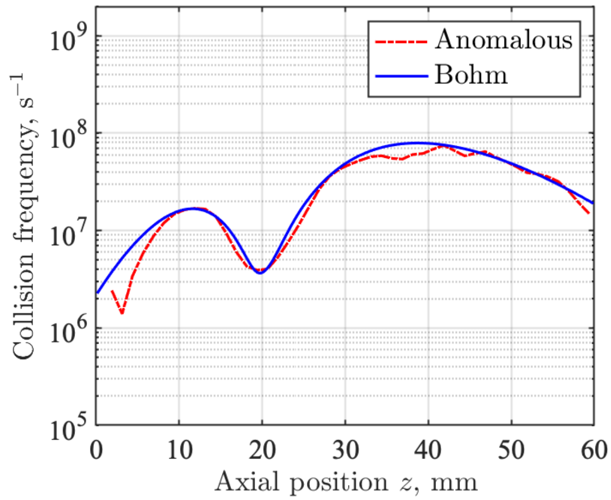

Figure 13. Approximation of the anomalous collision frequency obtained from the Z-θ simulation by the Bohm diffusion model. The Bohm diffusion coefficient is defined by Eq. (16).

V.D. Approximation by the Bohm Diffusion Model

The anomalous electron transport property obtained by the Z-θ simulation is utilized in the Z-R simulation through the Bohm diffusion model. The Bohm diffusion model is defined by the arbitrary Bohm diffusion coefficient α_B as written in Eq. (8). Here, the axial distribution of α_B is approximated by a Gaussian equation as follows:

$$\alpha_\mathrm{B} = (\alpha_\mathrm{p} - \alpha_0) \exp\left(-\frac{1}{2\sigma^2}\left(\frac{x}{x_\mathrm{p}} - 1\right)^2\right) + \alpha_0, \tag{16}$$

where the parameters are set as

$$\alpha_0 = 0.7, \qquad \alpha_\mathrm{p} = 0.022, \qquad x_\mathrm{p} = 20 \text{ mm}, \qquad \sigma = 0.43 \;\; (x \le x_\mathrm{p}), \quad \sigma = 0.55 \;\; (x > x_\mathrm{p}). \tag{17}$$

Figure 13 compares the simulated anomalous collision frequency and the Bohm diffusion model. The Bohm diffusion model well approximates the anomalous collision frequency. This Bohm diffusion model is used for the Z-R simulation.

V.E. Validation of Simulation Results

Empirical distributions of the effective electron mobility have been obtained for the SPT-type thrusters in preceding studies. To validate the simulated electron transport property, the effective electron mobility is compared between the present Z-θ simulation and the empirical distributions. Here the effective electron mobility data of the PPS-1350 and UM/AFRL P5 thrusters are taken from Refs. 30 and 5, respectively. Note that only a qualitative discussion is possible with this comparison, since the experimental data from different thrusters are used.

Figure 14 shows the results of the comparison. The horizontal axis corresponds to the axial position normalized by the channel length. The simulation result and the empirical data show similar trend as follows: 1) μ_eff is 10^1 to 10^2 m^{2}V^{-1}s^{-1} in the vicinity of the anode, 2) μ_eff has a minimum value of $\sim 10^{-1}$ m^{2}V^{-1}s^{-1} at around the channel exit, and 3) μ_eff is increased again to 10^0 to 10^1 m^{2}V^{-1}s^{-1} in the plume region. The "V-shaped" distribution of simulated μ_eff around the channel exit resembles the empirical data. Therefore, the anomalous electron transport property obtained in the Z-θ simulation qualitatively agrees with the empirical data, which increases the validity of the model.

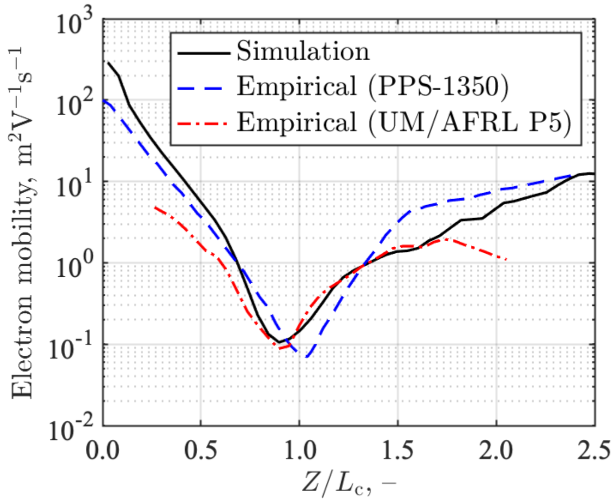

Figure 14. Comparison of effective electron mobilities between the simulation and empirical distributions. PPS-1350 and UM/AFRL P5 data are replotted from Refs. 30 and 5, respectively.

VI. Case SPT: Z-R Simulation

VI.A. Calculation Condition

A Z-R axisymmetric simulation is performed by using the anomalous electron transport property obtained by the Z-θ simulation. The Bohm diffusion coefficient defined in Eq. (16) is used in calculating the effective collision frequency in Eq. (8). The present hybrid model has been applied to the Z-R simulation of SPT-type thruster in the previous studies,[15,31] and the detail of the model can be found in the references. The calculation domain and boundary conditions are shown in Fig. 15. The calculation domain is rectangular with the size of 50 mm $\times$ 15 mm. Practical numerical simulations of Hall thrusters generally have wider calculation region in the plume for accurate thruster performance prediction. In this study, the main purpose of the Z-R simulation is to check the feasibility of simulation with the simulated anomalous electron property, and hence the simple rectangular region is taken for the simulation. Neutral particles of xenon corresponding to the mass flow rate are introduced into the calculation domain from the anode boundary of 40 mm$< R <$ 45 mm. The initial velocities of incident and reflected neutral particles are determined by the Maxwellian distribution and cosine law based on the channel wall temperature. A uniform rectangular grid of 70$\times$ 42 is applied in this study. The magnetic field geometry is assumed based on the figures in Ref. 27.

VI.B. Z-R Simulation Results

The Z-R simulation for the SPT case successfully ran as well as the TAL case. Time histories of the discharge current are presented in Fig. 16. The discharge is stable and the amplitude of the ionization oscillation is not

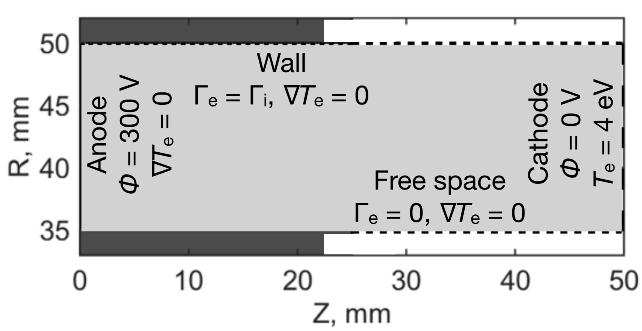

Figure 15. Calculation condition for the Z-R simulation (SPT case).

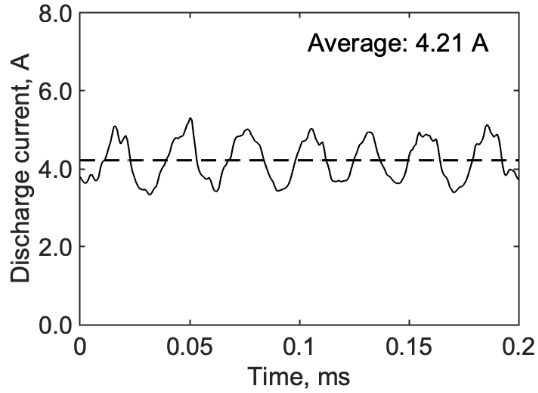

Figure 16. Time histories of discharge current calculated in the Z-R simulation for the SPT case.

Table 4. Comparison of thruster performance between the Z-R simulation and experiment.[27]

Parameter	Simulation	Experiment
Discharge current	4.21 A	4.5 A
Thurst	86.1 mN	90.2 mN
Anode efficiency	0.59	0.60

significant. The thruster performance predicted by the Z-R simulation is compared with the experimental results in Table 4. The simulated thruster performance agrees well with the experiment with the differences less than 10%. The agreement in the discharge current supports the validity of the anomalous electron transport property obtained in the Z-θ simulation.

Time-averaged plasma property distributions are shown in Fig. 17. The obtained profile are similar to the simulation results in preceding researches that used empirical electron transport models.[20,28] Especially the peak electron number density is 1.8×10^{18} m^{-3} in this simulation, and this value quantitatively agrees with the values in the preceding simulations. In addition to the TAL case, the Z-θ-Z-R simulation yields reasonable results for the SPT-100 case. It is demonstrated that the Z-θ-Z-R simulation can be one approach to the self-consistent Hall thruster discharge model.

VII. Conclusion

The coupled simulation of Z-θ and Z-R 2D hybrid models is proposed for the Hall thruster discharge modeling with a self-consistent electron transport model. Z-θ calculation simulates the azimuthal plasma oscillation to obtain the anomalous electron transport property. The obtained property is then used in the Z-R simulation. The purpose of the Z-R calculation is to simulate the thruster performance and magnetic field geometry effects. The feedback from the Z-R simulation to the Z-θ simulation is the ion wall flux distribution. The coupled Z-θ-Z-R simulation is applied to the TAL UT-58 and SPT-100 thrusters, to examine the applicability and validity of the model.

In the results of Z-θ simulation for the TAL case, azimuthal oscillations were observed in the ion number density and plasma potential distributions. Azimuthal electric field was induced especially at just downstream of the acceleration region. The cross-field electron transport was enhanced by the azimuthal plasma oscillation, especially in the plume region. In the plume region, the drift effect caused by the azimuthal gradients was predominant in the axial electron transport. Axial distribution of the effective electron mobility was evaluated and it was shown that the effective electron mobility was greater than the classical mobility by one to two orders of magnitude. Axial distribution of the simulated space potential showed a good agreement with the emissive prove measurement result. In addition, the mesh convergence was achieved when the number of azimuthal grid points was changed. These facts validate the anomalous electron transport property obtained by the Z-θ simulation.

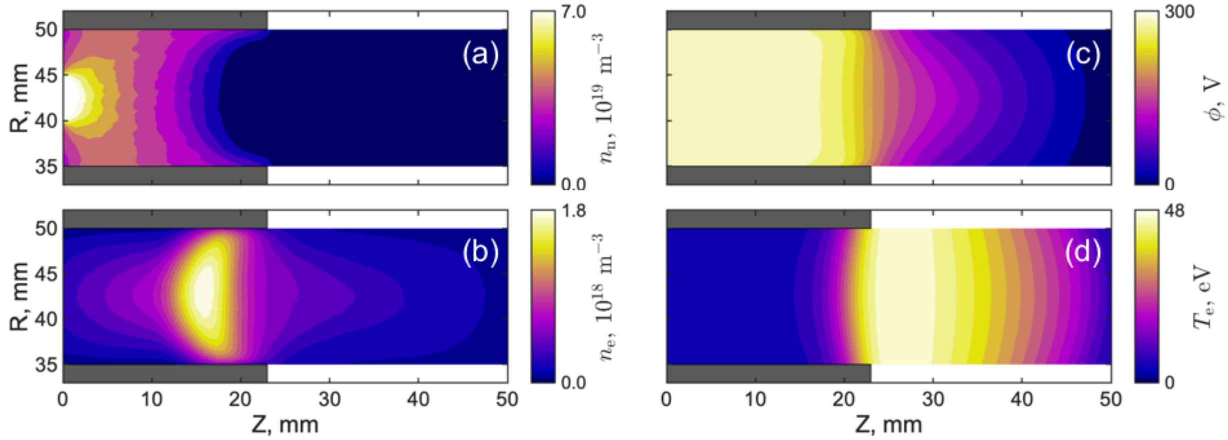

Figure 17. Plasma property distributions obtained from the Z-R simulation for the SPT case; (a) neutral number density, (b) ion number density, (c) space potential, and (d) electron temperature.

The Z-R simulation was performed by using the Bohm diffusion model that approximated the effective electron mobility in the Z-θ simulation results. The simulation successfully ran for a long time and a breathing-mode oscillation was observed in the results. The simulated discharge current was close to the measured value, which increased the confidence on the simulated property of the anomalous electron transport.

The Z-θ-Z-R simulation yielded reasonable simulation results for the SPT-100 case in addition to the TAL case. An azimuthal plasma oscillation was observed in the Z-θ simulation, and the cross-field electron transport was enhanced by the oscillation, around the channel exit and in the plume region. The anomalous collision frequency was well approximated by the Bohm diffusion model. The characteristics of effective electron mobility obtained from the simulation qualitatively agreed with the empirical distributions. The Z-R simulation for the SPT case also successfully ran with the Bohm diffusion model obtained by the Z-θ simulation. A quasi-steady state was achieved with a moderate breathing-mode oscillation. The thruster performance predicted by the Z-R simulation showed a good agreement with the experimental results. The Z-θ-Z-R simulation also showed its validity in the SPT case, in addition to the TAL case. It is demonstrated that the Z-θ-Z-R simulation can be one approach to the self-consistent Hall thruster discharge model.

References

[1]Funaki, I., Iihara, S., Cho, S., Kubota, K., Watanabe, H., Fuchigami, K., and Tashiro, Y., "Laboratory Testing of Hall Thrusters for All-electric Propulsion Satellite and Deep Space Explorers," 52nd AIAA/SAE/ASEE Joint Propulsion Conference, AIAA 2016-4942, 2016.

[2]Mikellides, I. G., Lopez Ortega, A., Hofer, R. R., Polk, J. E., Kamhawi, H., Yim, J. T., and Myers, J., "Hall2De Simulations of a 12.5-kW Magnetically Shielded Hall Thruster for the NASA Solar Electric Propulsion Technology Demonstration Mission Hall2De Simulations of a 12.5-kW Magnetically Shielded Hall Thruster for the NASA Solar Electric Propulsion Technology Demonstration Mission," 34th International Electric Propulsion Conference, IEPC-2015-254, 2015.

[3]Hamada, Y., Bak, J., Kawashima, R., and et al., "Hall Thruster Development for Japanese Space Propulsion Programs," *Trans. Japan Soc. Aero. Space Sci.*, Vol. 60, No. 5, 2017, pp. 320–326.

[4]Boeuf, J.-P., "Tutorial: Physics and modeling of Hall thrusters," *Journal of Applied Physics*, Vol. 121, No. 1, 2017, pp. 011101.

[5]Koo, J. W. and Boyd, I. D., "Modeling of anomalous electron mobility in Hall thrusters," *Physics of Plasmas*, Vol. 13, No. 3, 2006, pp. 033501.

[6]Hagelaar, G. J. M., Bareilles, J., Garrigues, L., and Boeuf, J. P., "Role of anomalous electron transport in a stationary plasma thruster simulation," *Journal of Applied Physics*, Vol. 93, No. 1, 2002, pp. 67–75.

[7]Anders, A., Ni, P., and Rauch, A., "Drifting localization of ionization runaway: Unraveling the nature of anomalous transport in high power impulse magnetron sputtering," *Journal of Applied Physics*, Vol. 111, No. 5, 2012, pp. 053304.

[8]Hirakawa, M. and Arakawa, Y., "Numerical simulation of plasma particle behavior in a Hall thruster," 32nd Joint Propulsion Conference and Exhibit, AIAA 1996-3195, 1996.

[9]Hirakawa, M., "Electron Transport Mechanism in a Hall Thruster," 25th International Electric Propulsion Conference, IEPC-97-021, 1997.

[10]Ortega, A. L., Katz, I., and Chaplin, V. H., "A First-Principles Model Based on Saturation of the Electron Cyclotron

Drift Instability for Electron Transport in Hydrodynamics Simulations of Hall Thruster Plasmas," 35th International Electric Propulsion Conference, IEPC-2017-178, 2017.

[11]Goebel, D. M. and Katz, I., *Fundamentals of electric propulsion: ion and Hall thrusters*, Vol. 2, John Wiley and Sons, 2008.

[12]Komurasaki, K. and Arakawa, Y., "Two-dimensional numerical model of plasma flow in a Hall thruster," *Journal of Propulsion and Power*, Vol. 11, No. 6, 1995, pp. 1317 – 1323.

[13]Fernandez, E., Dowdy, C., and Aley, J., "Characterization of Fluctuations in Hybrid Axial-Azimuthal Hall Thruster Simulations," 34th International Electric Propulsion Conference, IEPC-2015-313, 2015.

[14]Kawashima, R., Komurasaki, K., and Schönherr, T., "A hyperbolic-equation system approach for magnetized electron fluids in quasi-neutral plasmas," *Journal of Computational Physics*, Vol. 284, 2015, pp. 59–69.

[15]Kawashima, R., Komurasaki, K., Schönherr, T., and Koizumi, H., "Magnetized Electron Flow Calculation Using a Hyperbolic System," 54th AIAA Aerospace Science Meeting, AIAA 2016-2159, 2016.

[16]Kawashima, R., Hara, K., Komurasaki, K., and Koizumi, H., "A Unified Model for Axial-Radial and Axial-Azimuthal Hall Thruster Simulations," 52nd Joint Propulsion Conference and Exhibit, AIAA 2016-4726, 2016.

[17]Nishida, H. and Nonomura, T., "ADI-SGS scheme on ideal magnetohydrodynamics," *Journal of Computational Physics*, Vol. 228, No. 9, 2009, pp. 3182 – 3188.

[18]Dugan, J. J. and Sovie, R., "Volume Ion Production Costs in Tenuous Plasmas: a General Atom Theory and Detailed Results for Helium, Argon, and Cesium," NASA Technical Note, D-4150, 1967.

[19]Hofer, R. R., Katz, I., Mikellides, I. G., Goebel, D. M., and Jameson, K. K., "Efficacy of Electron Mobility Models in Hybrid-PIC Hall Thruster Simulations," 44th Joint Propulsion Conference and Exhibit, AIAA 2008-4924, 2007.

[20]Kubota, K., Cho, S., Watanabe, H., and Funaki, I., "Hybrid-PIC Simulation of Hall Thruster with Internally Mounted Cathode," 35th International Electric Propulsion Conference, IEPC-2017-429, 2017.

[21]Fujita, D., Kawashima, R., Ito, Y., Akagi, S., Suzuki, J., Schönherr, T., Koizumi, H., and Komurasaki, K., "Operating parameters and oscillation characteristics of an anode-layer Hall thruster with argon propellant," *Vacuum*, Vol. 110, 2014, pp. 159–164.

[22]Kawashima, R., Hara, K., and Komurasaki, K., "Numerical analysis of azimuthal rotating spokes in a crossed-field discharge plasma," *Plasma Sources Science and Technology*, Vol. 27, No. 3, 2018, pp. 035010.

[23]Boeuf, J. P., "New insights from PIC simulations on the EXB Electron Drift Instability in Hall thrusters," 35th International Electric Propulsion Conference, IEPC-2017-216, 2017.

[24]Esipchuk, Y. B. and Tilinin, G. N., "Drift Instability in a Hall-Current Plasma Accelerator," *Soviet Physics. Technical Physics*, Vol. 21, 1976, pp. 417.

[25]Frias, W., Smolyakov, A. I., Kaganovich, I. D., and Raitses, Y., "Long wavelength gradient drift instability in Hall plasma devices. I. Fluid theory," *Physics of Plasmas*, Vol. 19, No. 7, 2012, pp. 072112.

[26]Bak, J., Kawashima, R., Komurasaki, K., and Koizumi, H., "Plasma formation and cross-field electron transport induced by azimuthal neutral inhomogeneity in an anode layer Hall thruster," *Physics of Plasmas*, Vol. 26, No. 7, 2019, pp. 073505.

[27]Mitrofanova, O. A., Gnizdor, R. Y., and Murashko, V. M., "New Generation of SPT-100," 32nd International Electric Propulsion Conference, IEPC-2011-041, 2011.

[28]Hofer, R., Mikellides, I., Katz, I., and Goebel, D., "Wall Sheath and Electron Mobility Modeling in Hybrid-PIC Hall Thruster Simulations," 43rd Joint Propulsion Conference and Exhibit, AIAA 2007-5267, 2007.

[29]Reid, B. M. and Gallimore, A. D., "Review of Hall Thruster Neutral Flow Dynamics," 30th International Electric Propulsion Conference, IEPC-2007-038, 2007.

[30]Lafleur, T., Baalrud, S. D., and Chabert, P., "Theory for the anomalous electron transport in Hall effect thrusters. II. Kinetic model," *Physics of Plasmas*, Vol. 23, No. 5, 2016, pp. 053503.

[31]Kawashima, R., Komurasaki, K., Schönherr, T., and Koizumi, H., "Hybrid Modeling of a Hall Thruster Using Hyperbolic System of Electron Conservation Laws," 34th International Electric Propulsion Conference, IEPC-2015-206, 2015.